Electronic Supplementary Material (ESI) for Chemical Communications

Electronic Supplementary Information

Towards Longer-Lived Metal-to-Ligand Charge Transfer States of Iron(II) Complexes: An *N*-Heterocyclic Carbene Approach**

Yizhu Liu, Tobias Harlang, Sophie E. Canton, Pavel Chábera, Karina Suárez-Alcántara, André Fleckhaus, Dimali A. Vithanage, Erik Göransson, Alice Corani, Reiner Lomoth, Villy Sundström, and Kenneth Wärnmark**

Table of Contents

1. Synthesis and structure identification

General

All the reactions were carried out using the standard Schlenk technique or in a glovebox. Anhydrous THF was obtained from a Braun SPS-800 system. Precoated Merck silica gel 60 F_{254} plates were used for TLC analysis. Flash column chromatography was performed on silica gel (Davisil 35-70 μm). Size-exclusion chromatography was performed on BioBeads S-X1 gel (Bio-Rad, column size ϕ 30×1200 mm). ^{1}H and ^{13}C NMR were recorded on a Bruker Avance 400 NMR spectrometer. Chemical shifts (δ) are reported relative to the shift-scale calibrated with the residual NMR solvent peak; CD_3CN (1.94 ppm for ^{1}H NMR and 1.32 and 118.26 ppm for ^{13}C NMR).[1] Electron spray ionization–high resolution mass (ESI–HRMS) spectra were recorded on a Waters Micromass Q-Tof micro mass spectrometer. Elemental analysis was performed by Mikroanalytisches Laboratorium KOLBE (Mülheim an der Ruhr, Germany). Common solvents including THF, CH_3CN, and diethyl ether were purchased from Honeywell and used as received. Ammonia, ammonium hexafluorophosphate, 2,6-dibromopyridine were purchased from Acros. Glyoxal, formaldehyde, *tert*-butylamine, anhydrous iron(II) bromide, 2,2':6',2"-terpyridine, and potassium *tert*-butoxide (1 M solution in THF) were purchased from Aldrich. 2,6-Bis(3-methylimidazolium-1-yl)pyridine dibromide was purchased from TCI. *N*-*tert*-butylimidazole,[2] 2,6-bis(3-*tert*-butylimidazolium-1-yl)pyridine dibromide,[3] and **3**[4] were synthesized according to literature procedure.

Bis(2,6-bis(3-methylimidazol-1-ylidene)pyridine)iron(II) hexafluorophosphate (1). In a 50-mL Schlenk tube 2,6-bis(3-methylimidazolium-1-yl)pyridine dibromide (1 mmol) was suspended in 15 mL of dry THF and cooled down to −78°C. *t*BuOK (1.2 mL, 1 M in THF) was then added and the mixture was stirred for 30 min at this temperature. The cooling bath was removed and 10 mL THF solution of anhydrous $FeBr_2$ (0.46 mmol) was dropped inside with a syringe before the mixture was warmed to room temperature. It was then further stirred in the dark overnight and filtered through a pad of Celite®. The collected solid was extracted with CH_3CN and the filtrate was evaporated. The residual was re-dissolved in a small amount of water, filtered over a pad of Celite®, and precipitated with NH_4PF_6 aqueous solution (1.3 g/10 mL). The *N*-methyl group exerted less protection to the coordination sphere, and **1** was found to be unstable on a silica gel column. Therefore, the crude product was purified twice by size-exclusion chromatography on BioBeads S-X1 using CH_3CN (40)/toluene (60) as eluent, and re-precipitated over CH_3CN/diethyl ether to give a brown yellow solid (201 mg, 53%). Single crystals suitable for X-ray diffraction were grown by slow diffusion of diethyl ether into the CH_3CN solution of the product. ^{1}H NMR (400 MHz, CD_3CN) δ (ppm) 8.17 (t, *J*=7.5 Hz, 2H), 8.00 (d, *J*=1.5 Hz, 4H), 7.72 (d, *J*=6.0 Hz, 4H), 6.99 (d, *J*=1.8 Hz, 4H), 2.50 (s, 12H). ^{13}C NMR (100.3 MHz, CD_3CN) δ (ppm) 201.20, 155.01, 139.31, 127.43, 117.33, 106.27, 35.41. ESI–HRMS: calc. for $[\mathbf{1}-(PF_6)]^+$ 679.1333, found 679.1353. Elemental analysis: calc. for $\mathbf{1}\cdot 1.5H_2O$ ($C_{26}H_{29}F_{12}FeN_{10}O_{1.5}P_2$) C, 36.68; H, 3.43; N, 16.45; found C, 36.90; H, 3.51; N, 16.14.

---

[1] G. R. Fulmer, A. J. M. Miller, N. H. Sherden, H. E. Gottlieb, A. Nudelman, B. M. Stoltz, J. E. Bercaw, K. I. Goldberg, *Organometallics* **2010**, *29*, 2176-2179.
[2] J. Liu, Z. Ren, Y. Zhao, H. Zhang, *Chin. J. Org. Chem.* **2004**, *24*, 1091-1094.
[3] D. J. Nielsen, K. J. Cavell, B. W. Skelton, A. H. White, *Inorg. Chim. Acta* **2006**, *359*, 1855-1869.
[4] C. M. Harris, H. R. H. Patil, E. Sinn, *Inorg. Chem.* **1969**, *8*, 101-104.

Bis(2,6-bis(3-*tert*-butylimidazol-1-ylidene)pyridine)iron(II) hexafluorophosphate (2). **2** was synthesized in a similar way as **1**, except that the *in-situ* deprotonation of the imidazolium salt was carried out at −15°C. The crude product after precipitation by NH_4PF_6 was purified by silica gel flash column chromatography, first with CH_3CN (99)/aq. sat. KPF_6 (1) then with THF (60)/THF sat. KPF_6 (40) as eluents. The collected fraction was evaporated, triturated with distilled H_2O, and re-precipitated over CH_3CN/diethyl ether to give orange solids (251 mg, 55%). Single crystals suitable for X-ray diffraction were grown by slow diffusion of diethyl ether into the CH_3CN–THF solution of the product. ^{1}H NMR (400 MHz, CD_3CN) δ (ppm) 8.30 (t, *J*=6.0 Hz, 2H), 8.14 (d, *J*=1.8 Hz, 4H), 7.93 (d, *J*=6.0 Hz, 4H), 7.41 (d, *J*=1.8 Hz, 4H), 0.72 (s, 36H). ^{13}C NMR (100.3 MHz, CD_3CN) δ (ppm) 190.72, 157.29, 140.61, 126.59, 117.06, 108.33, 58.94, 30.59. ESI–HRMS: calc. for $[\mathbf{2}-(PF_6)]^+$ 847.3211, found 847.3214. Elemental analysis: calc. for **2** ($C_{38}H_{50}F_{12}FeN_{10}P_2$) C, 45.98; H, 5.08; N, 14.11; found C, 45.93; H, 5.07; N, 14.12.

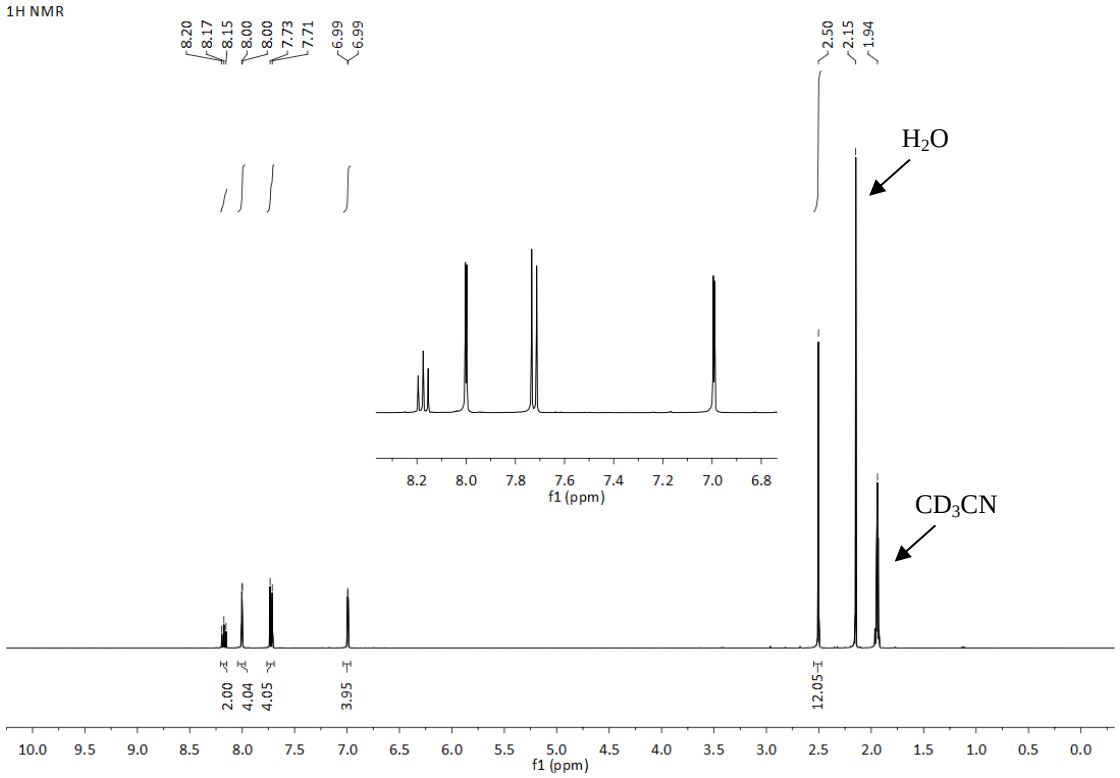

Figure S1. ^{1}H NMR of **1** in CD_3CN.

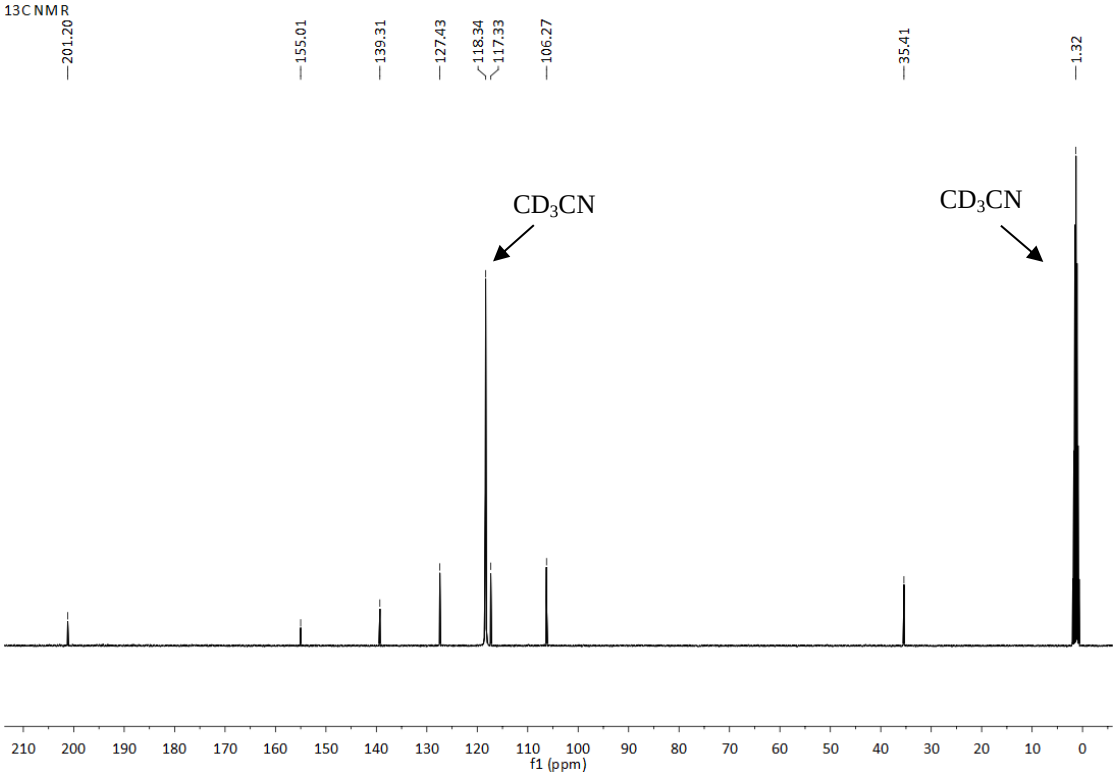

Figure S2. ^{13}C NMR of **1** in CD_3CN.

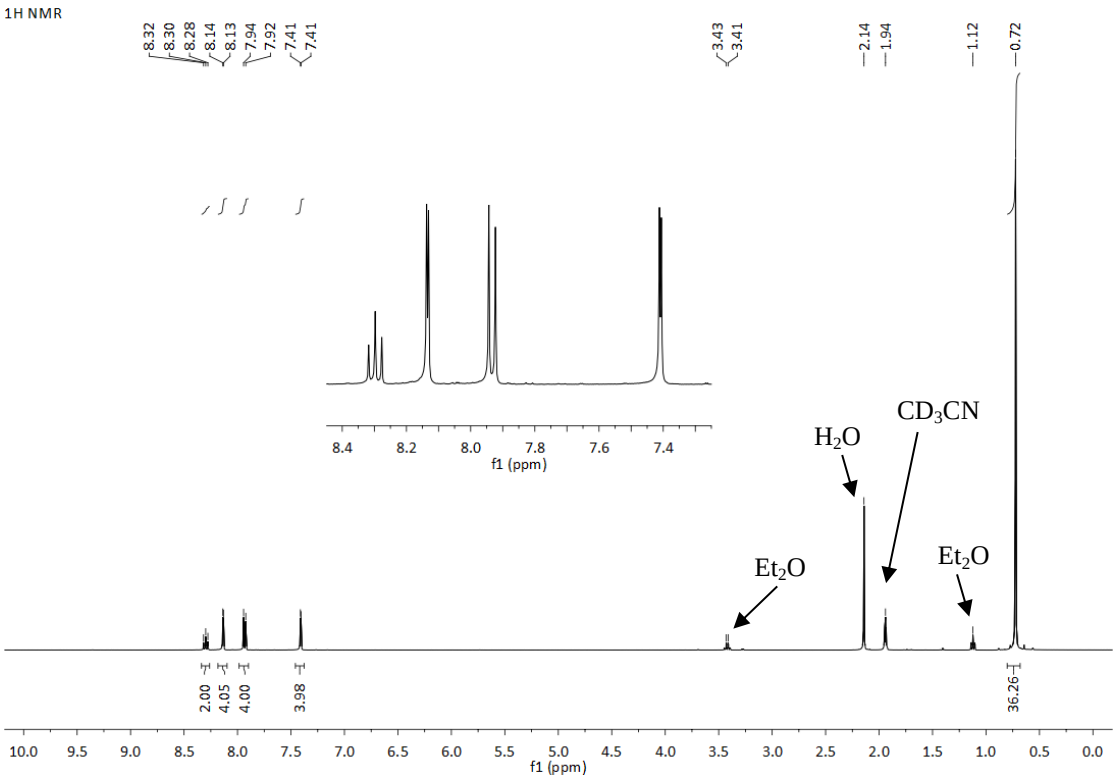

Figure S3. ^{1}H NMR of **2** in CD_3CN.

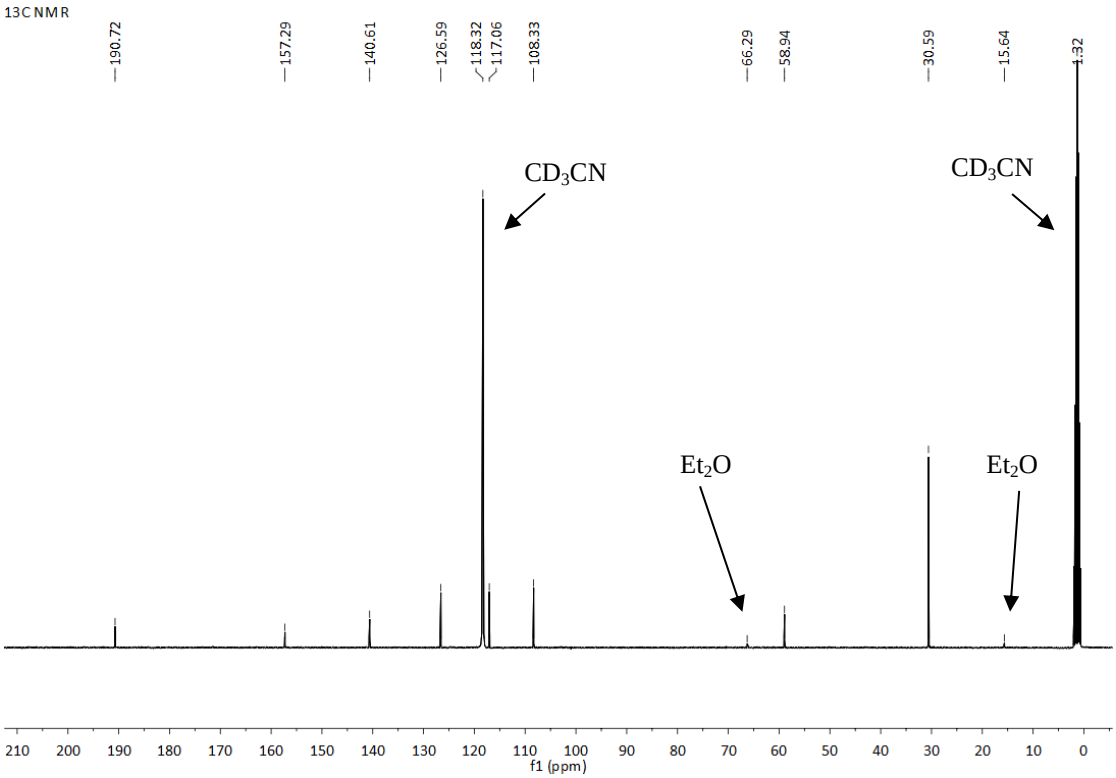

Figure S4. ^{13}C NMR of **2** in CD_3CN.

2. Crystallographic data of 1 and 2

Single crystals suitable for X-ray diffraction were grown by slow diffusion of diethyl ether into the CH_3CN solution of **1** or CH_3CN/THF solution of **2**. Intensity data for **1** and **2** were collected at 293 K with an Oxford Diffraction Xcalibur™ 3 system using ω-scans and Mo-Kα radiation (Λ = 0.71073 Å).[5] CCD data were extracted, integrated and the absorptions were corrected by a multi-scan method using Crysalis RED.[6] Both structures were solved by direct methods and refined by full-matrix least-squares calculations on F^2 using SHELXTL 6.14[7] and WinGX 1.80.05.[8] Non-H atoms were refined with anisotropic displacement parameters. Hydrogen atoms were constrained to parent sites, using a riding model. All crystallographic data is available in CIF format, and can be obtained free of charge from The Cambridge Crystallographic Data Centre via www.ccdc.cam.ac.uk/data_request/cif. CCDC reference numbers are 915795 (**1**) and 915796 (**2**).

The structures of both compounds **1** and **2** contained disordered solvent molecules. Attempts to suppress those electron densities using a SQUEEZE procedure[9] did not lead to decreasing difference Fourier peaks.

The structure of **1** contains one molecule of acetonitrile in the asymmetric unit. The positions are only partially occupied. For a stable refinement no hydrogen atoms were added to this molecule.

The structure of **2** contains two molecules of THF in the asymmetric unit. One of the solvent molecules refines as expected leading to a reasonable structure while the other solvent molecule refines to a disordered 5-membered ring with very small C–C distances. For a stable refinement no hydrogen atoms were added to the latter.

Crystal data for **1**: C52.82 H52 F24 Fe2 N20.40 P4, M = 1664.73, monoclinic, space group = P21/n (#14), a = 20.2230(6) Å, b = 11.5332(3) Å, c = 29.2642(8) Å, β = 98.996(3)°, V = 6741.5(3) Å^3, Z = 4, density (calc.) = 1.640, independent reflections = 16747 (Rint = 0.0558), GOF = 1.056. The final R1 factor was 0.0680 (I>2σ(I)) (wR2 = 0.1727).

Crystal data for **2**: C84 H108 F24 Fe2 N20 O2 P4, M = 2121.48, triclinic, space group = P-1 (#2), a = 12.8044(5) Å, b = 20.5091(5) Å, c = 20.5285(6) Å, α = 95.655(3)°, β = 95.655(3)°, γ = 90.690(3)°, V = 4954.0(3) Å^3, Z = 2, density (calc.) = 1.422, independent reflections = 23760 (Rint = 0.0461), GOF = 1.028. The final R1 factor was 0.0668 (I>2σ(I)) (wR2 = 0.1956).

---

[5] *Crysalis CCD*, Oxford Diffraction Ltd. Abingdon, Oxfordshire, UK, 2005.
[6] *Crysalis RED*, Oxford Diffraction Ltd. Abingdon, Oxfordshire, UK, 2005.
[7] G.M. Sheldrick. *Acta Cryst.* **2008**, A64, 112-122.
[8] L.J Farrugia, *J. Appl. Cryst.* **1999**, *32*, 837-838.
[9] A.L. Spek, *Acta Cryst.* **2009**, D65, 148-155.

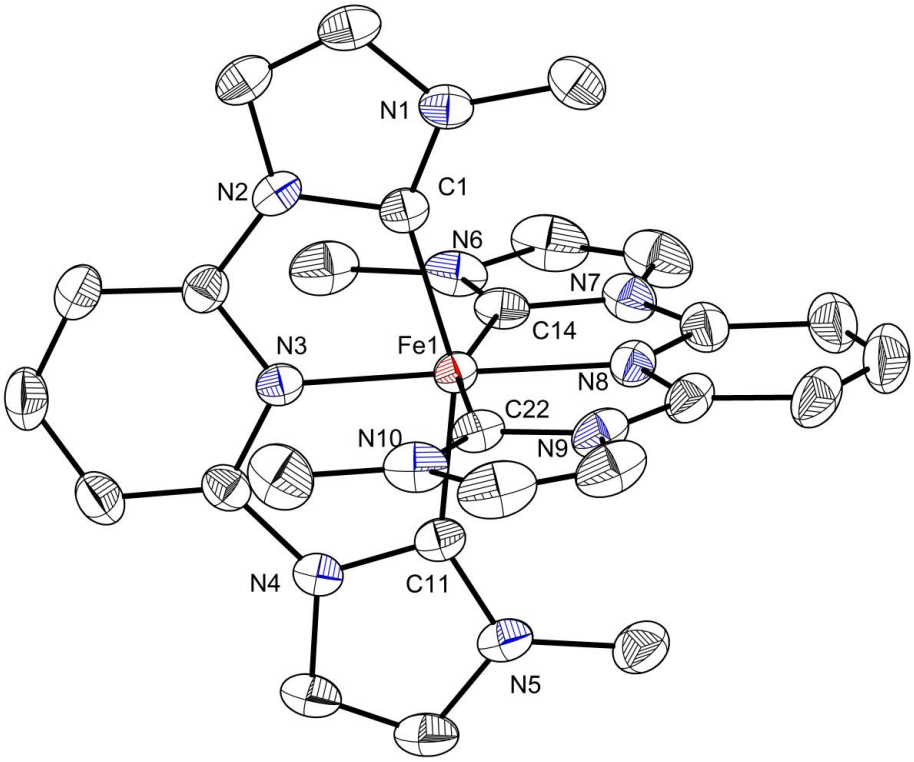

Figure S5. Molecular structure of **1** (anisotropic displacement ellipsoids set at 30% probability). Hydrogen atoms, counter-ions, and solvent of crystallization have been omitted for clarity.

Table S1. Selected bond lengths [Å] and angles [°] for **1**.

Fe1–C1	1.966(3)	C1–Fe1–N3	79.5(1)
Fe1–N3	1.919(3)	C11–Fe1–N3	79.2(1)
Fe1–C11	1.965(3)	C1–Fe1–C11	158.6(2)
Fe1–C14	1.965(3)	C14–Fe1–N8	79.0(1)
Fe1–N8	1.930(3)	C22–Fe1–N8	79.0(1)
Fe1–C22	1.970(3)	C14–Fe1–C22	158.0(2)
C1–N1	1.335(5)	N3–Fe1–N8	178.6(1)
C1–N2	1.392(5)	N1–C1–N2	103.4(3)
C11–N4	1.391(5)	N4–C11–N5	103.5(3)
C11–N5	1.349(5)	N6–C14–N7	103.7(3)
C14–N6	1.342(4)	N9–C22–N10	103.7(3)
C14–N7	1.395(5)		
C22–N9	1.383(5)		
C22–N10	1.344(5)		

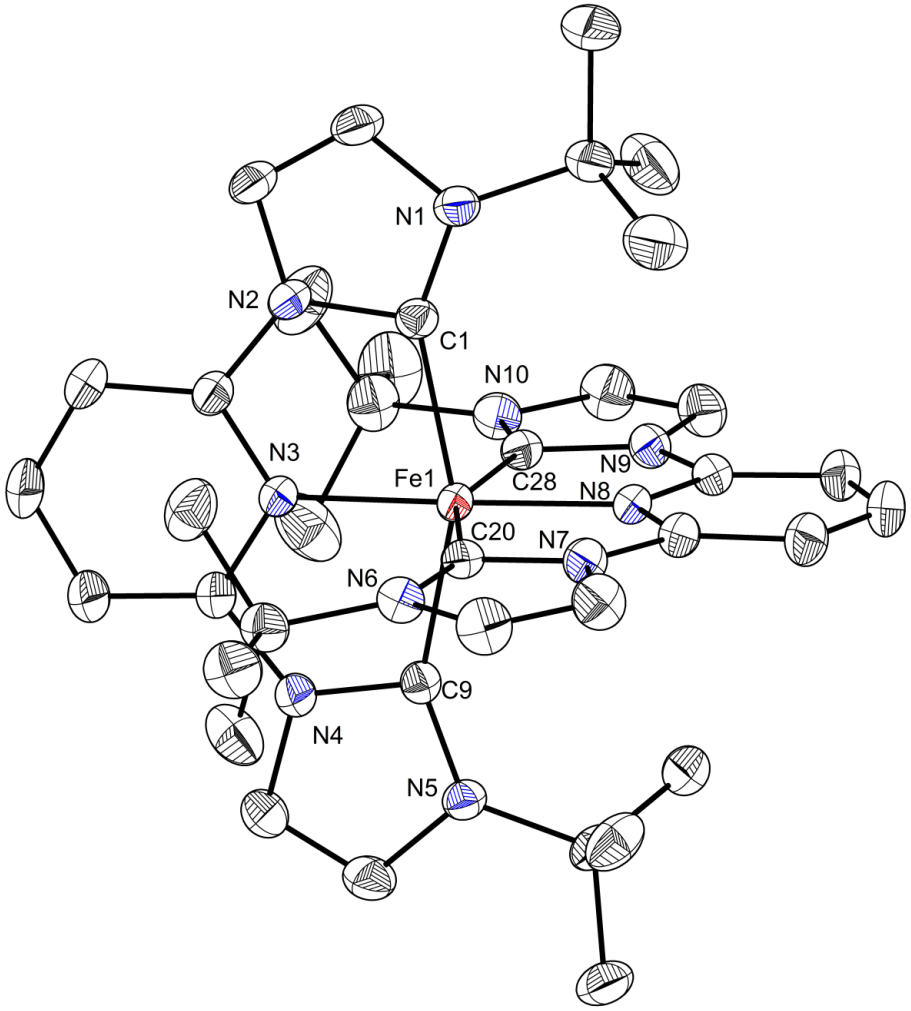

Figure S6. Molecular structure of **2** (anisotropic displacement ellipsoids set at 30% probability). Hydrogen atoms, counter-ions, and solvent of crystallization have been omitted for clarity.

Table S2. Selected bond lengths [Å] and angles [°] for **1**.

Fe1–C1	2.104(3)	C1–Fe1–N3	79.3(1)
Fe1–N3	1.936(3)	C9–Fe1–N3	78.9(1)
Fe1–C9	2.083(3)	C1–Fe1–C9	158.2(1)
Fe1–C20	2.088(3)	C20–Fe1–N8	78.8(1)
Fe1–N8	1.941(2)	C28–Fe1–N8	79.0(1)
Fe1–C28	2.108(2)	C20–Fe1–C28	157.8(1)
C1–N1	1.378(4)	N3–Fe1–N8	178.7(1)
C1–N2	1.396(4)	N1–C1–N2	101.9(2)
C9–N4	1.396(4)	N4–C9–N5	101.7(2)
C9–N5	1.375(4)	N6–C20–N7	102.0(2)
C20–N6	1.385(3)	N9–C28–N10	102.2(2)
C20–N7	1.393(4)		
C28–N9	1.385(4)		
C28–N10	1.377(4)		

3. Cyclic voltammetry, spectroelectrochemistry, and simulation of differential absorption spectra

All samples were dissolved in CH_3CN (Merck, spectroscopic grade, dried with 3 Å molecular sieves) with *n*-Bu_4NPF_6 (TBAH, Fluka, electrochemical grade, vacuum dried at 383 K) as supporting electrolyte (0.1 M). All solutions were deaerated by bubbling with solvent-saturated argon and kept under argon atmosphere during measurements.

Cyclic voltammetry (scan rate 0.1 V/s) was performed in a three-electrode, three-compartment cell controlled by an Autolab potentiostat (PGSTAT 302) with a GPES electrochemical interface (Eco Chemie). The cell was equipped with a glassy carbon disk working electrode (diam. 1 mm, CH Instruments), a glassy carbon rod auxiliary electrode, and a non-aqueous Ag^+/Ag reference electrode (CH Instruments, 0.010 M $AgNO_3$ in acetonitrile) with a potential of −0.08 V vs. the ferrocenium/ferrocene (Fc^+/Fc) couple in acetonitrile as an external standard. Potential values for reversible processes reported in this work were calculated as the average of the oxidative and reductive peak potentials ($E_{p,a}$ + $E_{p,c}$)/2, while those for irreversible processes (the one-electron reduction of **1** and **2**) were reported directly.

Table S3. Steady-state absorption and redox properties of **1**-**3**.

Complex	λ_{max}/nm (ε/10^4 M^{-1} cm^{-1})[a]	$E^{3+/2+}$/V[b] (ΔE_p/mV)	$E^{2+/+}$/V[b] (ΔE_p/mV)
1	457 (1.52), 390 (0.91), 286 (3.11), 244 (3.44)	+0.31 (60)	−2.39[c]
2	478 (1.48), 412 (0.84), 299 (3.09), 251 (3.84)	+0.40 (64)	−2.35[c]
3	552 (1.48), 495 (0.75, sh), 369 (0.54, sh), 319 (6.63), 280 (4.51), 273 (5.15)	+0.70 (67)	−1.66 (61)

[a] In CH_3CN. [b] In CH_3CN. Potential values referred to ferrocenium/ferrocene (Fc^+/Fc). [c] Irreversible peaks.

Spectroelectrochemistry was recorded on an 8453 UV-Vis diode array spectrophotometer (Agilent Technologies). The custom built three-electrode, three-compartment quartz cell with an optical path length of 1 mm was equipped with a Pt mesh working electrode and the same reference and auxiliary electrodes as described for cyclic voltammetry. Multiple spectra were recorded in the course of controlled potential electrolysis that generated the desired redox states of complex **3** and $[Ru^{II}(tpy)_2](PF_6)_2$ (tpy=2,2':6',2"-terpyridine, **Rutpy**). The spectra obtained after exhaustive electrolysis were used for generating simulated differential absorption spectra.

Optical excitation of **Rutpy** is known to result in the ^{3}MLCT state having roughly the same lifetime (~120 ps) as ground state bleach (GSB) recovery. [10] Therefore, a good matching between the optical differential absorption spectrum of **Rutpy** measured in transient absorption (TA) spectroscopy, and the spectroelectrochemically simulated differential absorption spectrum of $[Ru^{III}(tpy)(tpy)^{\bullet-}]^{2+}$ (theoretical electronic configuration in the ^{3}MLCT state of **Rutpy**) relative to its ground state, would validate spectroelectrochemistry as a trustable method of modeling the absorption of the ^{3}MLCT excited state. The simulated differential absorption spectrum was generated by adding the differential absorption spectra taken for both metal-based oxidation and ligand-based reduction processes.[11,12] The optical differential absorption spectrum was replotted according to ref. 10. Comparison of the two is shown in the bottom panel of Figure S5, from which a good agreement is clearly seen, as expected.

For **3**, basically the same procedure was followed. However, unlike **Rutpy**, the ^{3}MLCT state of **3** is very short-lived (~145 fs, see main text). Therefore, in **Rutpy**, ^{3}MLCT state and GSB are coupled with each other in a 1:1 molar ratio in most of the temporal range; whereas in **3**, even at early times, for example 0.25 ps delay time, there is already deactivation of ^{3}MLCT by $^5T_2$. The optical differential absorption spectrum measured at this time thus does not directly reflect the difference between ^{3}MLCT and ground state, as there is excess amount of GSB associated with newly formed $^5T_2$ state, distorting the differential spectrum with too large fraction of negative GSB signal. Considering that at 600 ps after excitation, only $^5T_2$ and GSB exist in a 1:1 molar ratio, and the absorption of $^5T_2$ is sufficiently weak, it is possible to correct the optical differential absorption spectrum at 0.25 ps after excitation by subtracting a weighted optical differential absorption spectrum at 600 ps. This is shown in the bottom panel of Figure S6, which is also in good agreement with the spectroelectrochemically simulated differential absorption spectrum.

[10] Y. Liu, R. Hammitt, D. A. Lutterman, R. P. Thummel, C. Turro, *Inorg. Chem.* **2007**, *46*, 6011-6021.
[11] J. E. Monat, J. K. McCusker, *J. Am. Chem. Soc.* **2000**, *122*, 4092-4097.
[12] A. L. Smeigh, M. Creelman, R. A. Mathies, J. K. McCusker, *J. Am. Chem. Soc.* **2008**, *130*, 14105-14107.

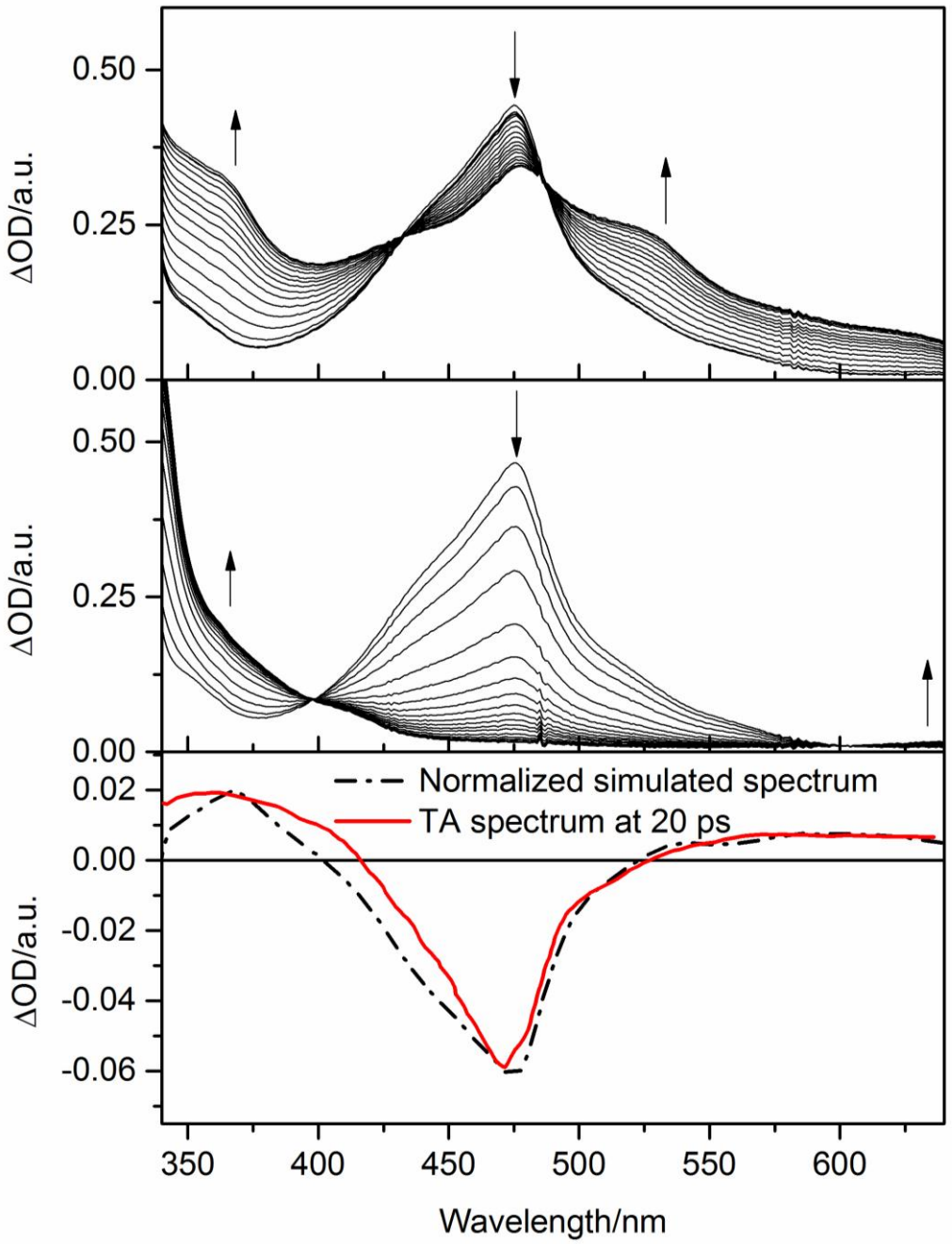

Figure S7. Top: spectroelectrochemistry of **Rutpy** recorded at −1.69 V vs. Fc^+/Fc; middle: spectroelectrochemistry of **Rutpy** recorded at +1.12 V vs. Fc^+/Fc; bottom: comparison of spectroelectrochemically simulated differential absorption spectrum (dash dot) with optical differential absorption spectrum measured in TA (red solid).

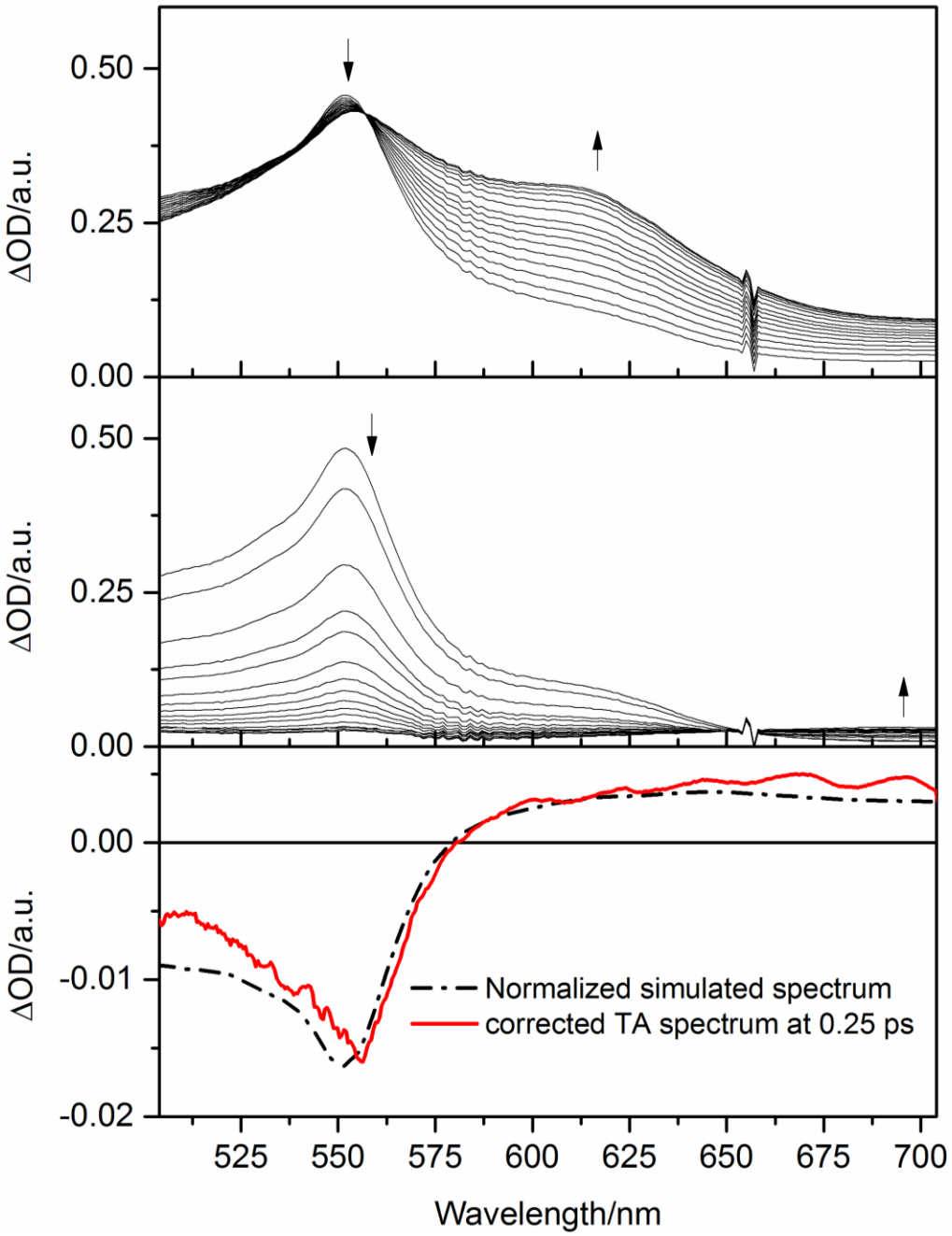

Figure S8. Top: spectroelectrochemistry of **3** recorded at −1.69 V vs. Fc^+/Fc; middle: spectroelectrochemistry of **3** recorded at +0.95 V vs. Fc^+/Fc; bottom: comparison of spectroelectrochemically simulated differential absorption spectrum (dash dot) with corrected optical differential absorption spectrum measured at 0.25 ps in TA (red solid).

4. Femtosecond transient absorption spectroscopy

The femtosecond laser setup is based on a MaiTai seeded Spitfire Pro XP amplifier (Spectra Physics) with central output wavelength of 795 nm and 1 kHz repetition rate delivering ~60 fs pulses. The beam was split into two parts: one for pumping a collinear optical parametric amplifier (TOPAS-C, Light Conversion) to generate the pump beam, while the second part was led through a computer-controlled delay line and used to generate the white-light continuum (WLC) probe. To generate the WLC the laser light was focused either into a 2-mm sapphire plate to probe the red part of transient spectra, or into a 3-mm CaF_2 translating optical window to probe in the blue-most tail of the transient spectrum. Subsequently, the probe pulses were split into two parts: the former overlapping with the pump pulse in the sample volume and the latter serving as a reference. The probe and the reference beams were then brought to the slit of a spectrograph and dispersed onto a double photodiode array, each with 512 elements (Pascher Instruments). The intensity of excitation pulses was kept below 5×10^{14} photons·pulse^{-1}·cm^{-2}. Steady-state absorption spectra were measured before and after experiments to make sure that sample degradation did not exceed 5% in any case (Figure S9). The mutual polarization between pump and probe beams was set to the magic angle (54.7°) by placing Berek compensator in the pump beam.

Global analysis[13,14] (the whole temporal range for **1**; from 4 ps for **2** and **3**) and one-dimensional fitting (from 0 to 4 ps, 530~640 nm for **2** and 580~700 nm for **3**, based on a damped oscillation superimposed on an exponential decay)[15] of the kinetics were performed according to literature procedures.

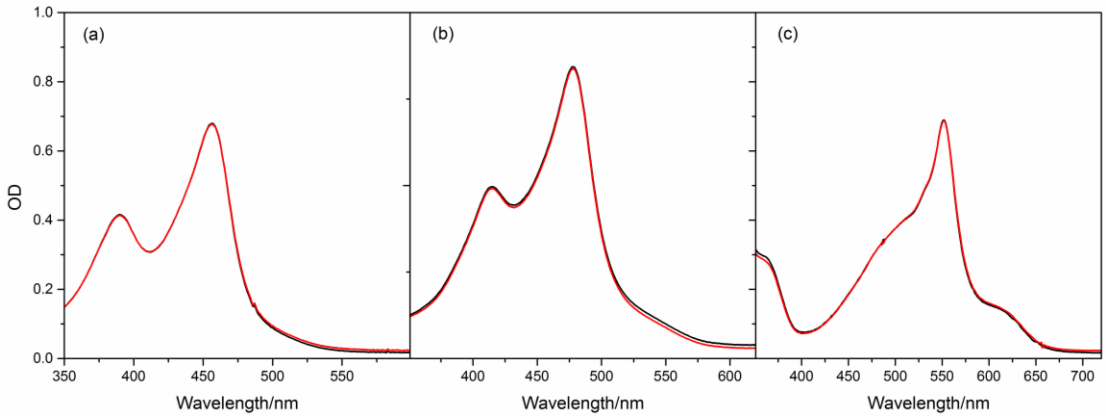

Figure S9. Steady-state absorption spectra of **1** (a), **2** (b), and **3** (c) in MeCN before (black) and after (red) the transient absorption measurement.

[13] I. H.M. van Stokkum, D. S. Larsen, R. van Grondelle, *Biochim. Biophys. Acta* **2004**, *1657*, 82-104.
[14] W. Gawelda, A. Cannizzo, V.-T. Pham, F. van Mourik, Ch. Bressler, M. Chergui, *J. Am. Chem. Soc.* **2007**, *129*, 8199-8206.
[15] C. Consani, M. Prémont-Schwarz, A. ElNahhas, Ch. Bressler, F. van Mourik, A. Cannizzo, M. Chergui, *Angew. Chem. Int. Ed.* **2009**, *48*, 7184-7187.

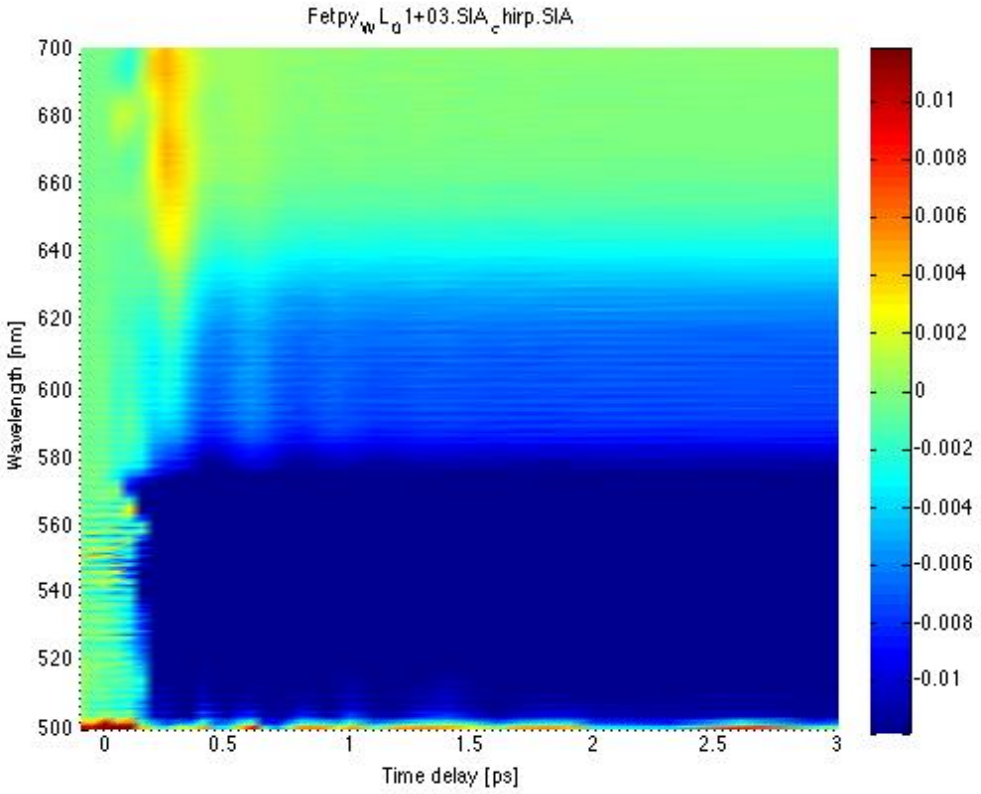

Figure S10. 2D wavelength–time plots of **3** in CH_3CN solution pumped at 485 nm, within first 3 ps.

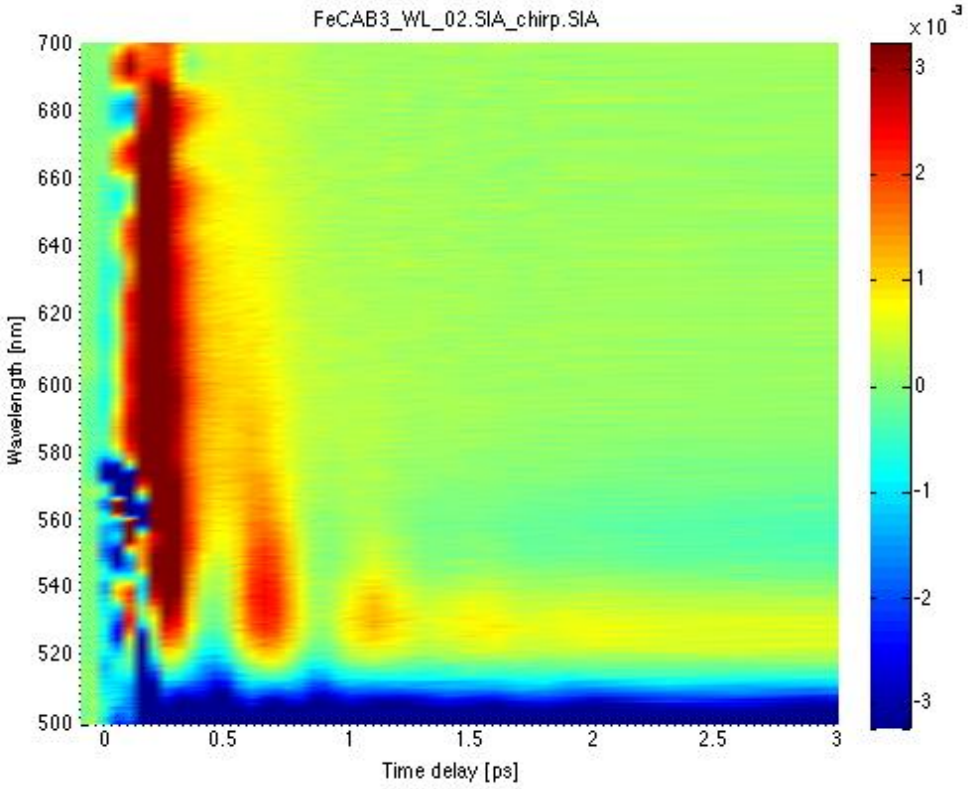

Figure S11. 2D wavelength–time plots of **2** in CH_3CN solution pumped at 485 nm, within first 3 ps.

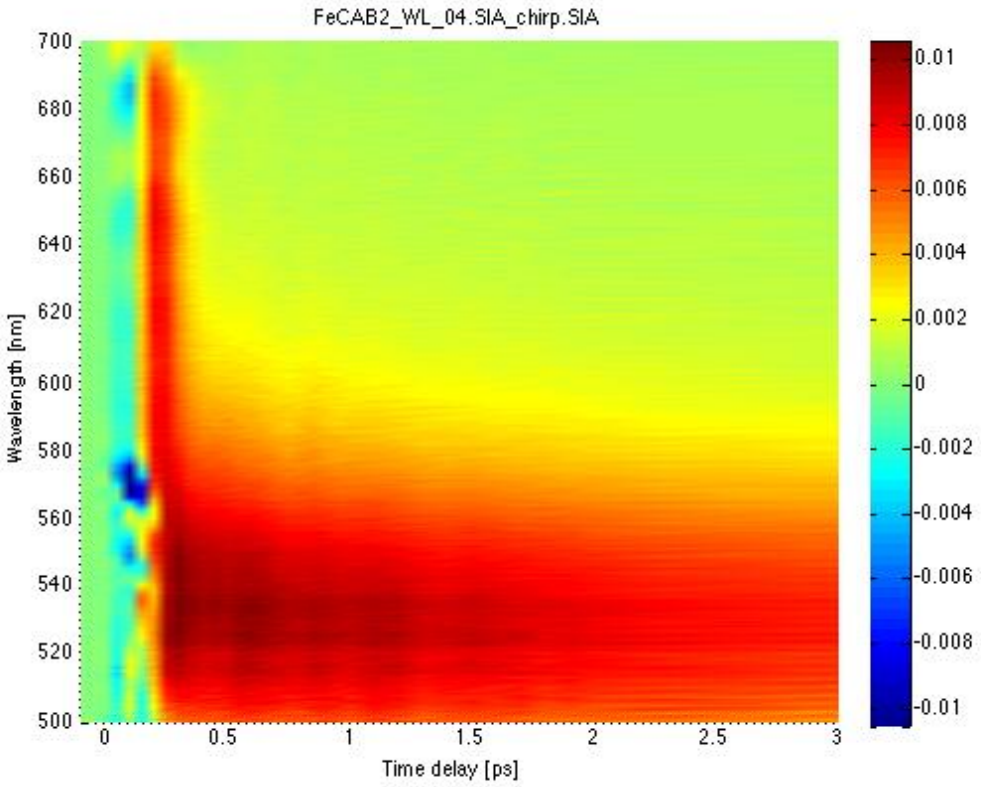

Figure S12. 2D wavelength–time plots of **1** in CH_3CN solution pumped at 485 nm, within first 3 ps.

For the one-dimensional fitting of the kinetics of **3**, throughout the wavelength range where this model is applicable, a constant oscillation period of 410±60 fs was extracted. At wavelengths longer than 660 nm, where the TA spectrum is dominated by ESA, a relatively constant exponential decay of 145±10 fs was obtained and assigned as the deactivation time of the ^{3}MLCT, which is similar to values reported for this class of complexes.[14,15] Recently, oscillations in the TA kinetics of the closely related $[Fe(bpy)_3]^{2+}$ (bpy=2,2'-bipyridine) were reported, and ascribed to vibrational wave packets in the HS state.[15] In our case, the oscillation is also likely to be related to the HS dynamics, and deeper investigations are in process.

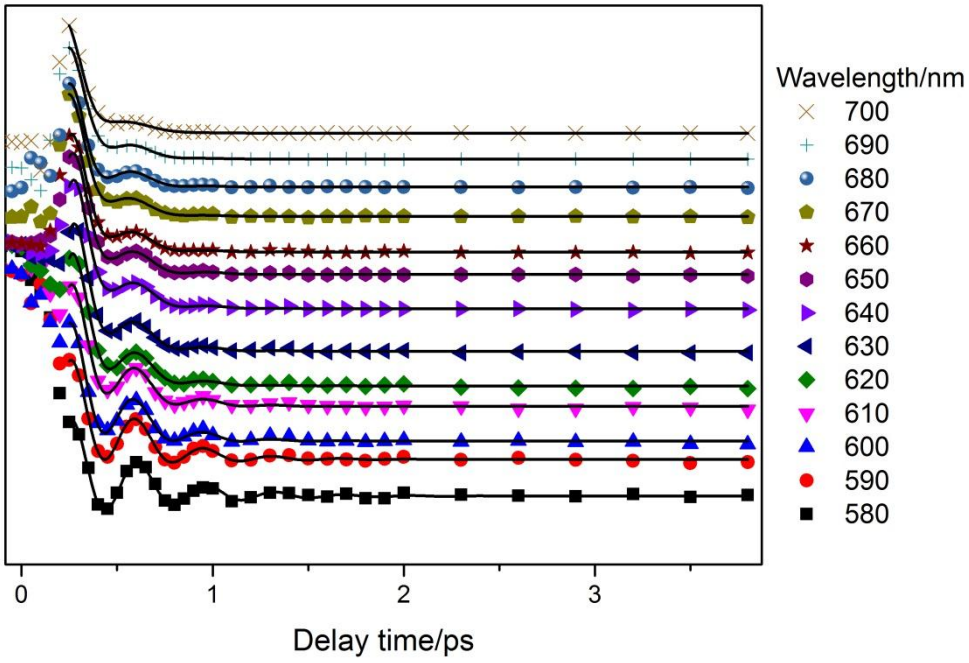

Figure S13. Fitting of the transient kinetics of **3** (580~700 nm) within the first 4 ps.

For **2**, transients above 660 nm, where little oscillation was noticed, were fitted with a bi-exponential function convoluted with IRF to give time constants of <100 and 330±20 fs. Transients between 520 and 660 nm can be well fitted using the same oscillation model, giving a constant oscillation period of 520±80 fs and an exponential decay of 200~300 fs. The lifetime of this decay component becomes somewhat uncertain below 570 nm due to the strong oscillations and the spectrally overlapping weak slower components (Figure 4c in the main text). Likewise, it is assigned as the deactivation time of the ^{3}MLCT.

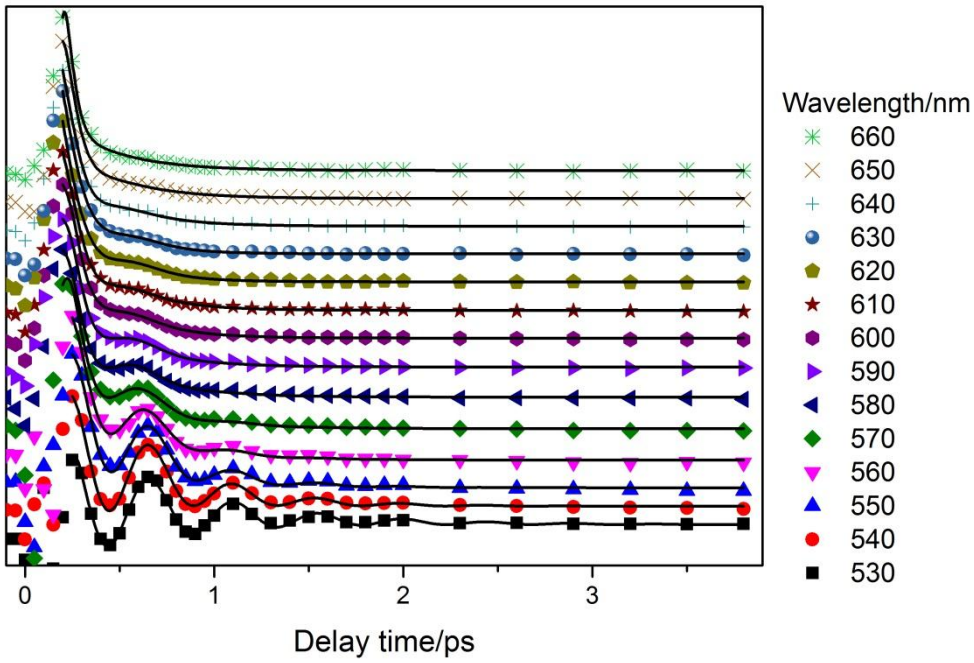

Figure S14. Fitting of the transient kinetics of **2** (530~660 nm) within the first 4 ps.

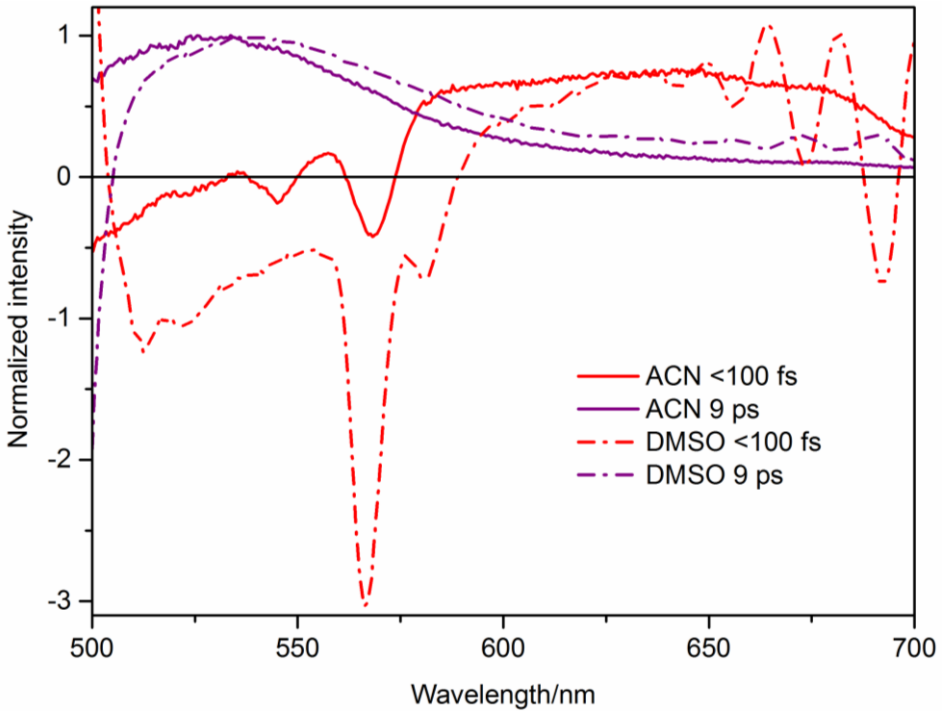

Figure S15. Normalized DAS of **1** in CH_3CN and DMSO.

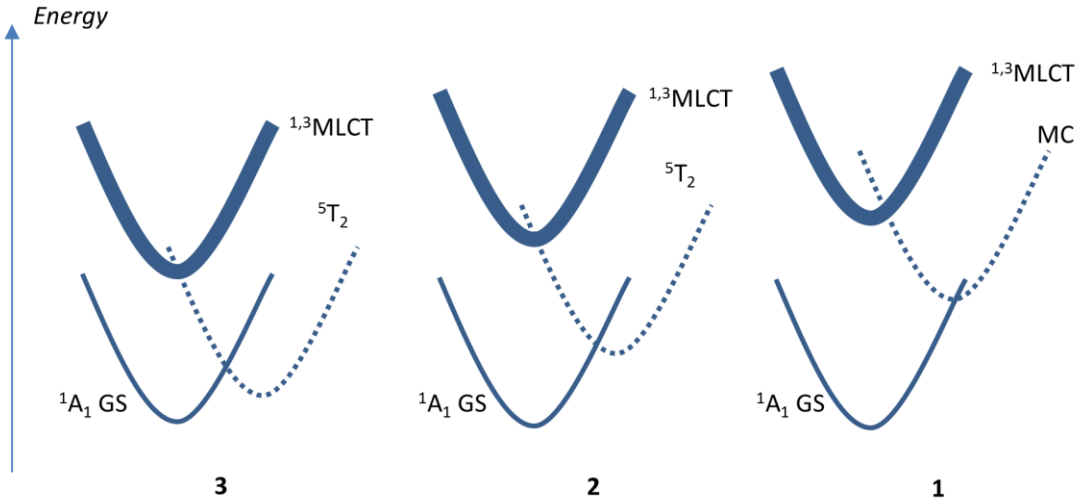

Figure S16. Tentative illustration of potential energy surface shifts and associated surface crossings through the series of studied molecules.

5. Emission properties of 1

Emission of **1** was not detected at either room temperature or 77 K. Flash photolysis measurements indicated that the ^{3}MLCT lifetime is <1 ns at 77 K. Assuming an emission rate constant of ~10^4 s^{-1}, commonly observed for $[RuN_6]^{2+}$ complexes,[16] the emission quantum yield of **1** is estimated to be <10^{-5}.

[16] A. Juris, V. Balzani, F. Barigelletti, S. Campagna, *Coord. Chem. Rev.* **1988**, *84*, 85-277.

6. Derivation of MC→^{1}A$_1$ relaxation time of 1

Assuming a sequential two-compartment mechanism of GSB recovery,

$$\mathrm{A} \xrightarrow{k_1} \mathrm{B} \xrightarrow{k_2} \mathrm{GS} \tag{1}$$

and the concentration of A right after the photoexcitation (in our case, assuming ^{3}MLCT is quantitatively populated from ^{1}MLCT) is A_0. The concentration of A as a function of time is

$$A(t) = A_0 e^{-k_1 t} \tag{2}$$

the rate of concentration change of B is

$$\frac{\mathrm{d}B(t)}{\mathrm{d}t} = k_1 A(t) - k_2 B(t) = k_1 A_0 e^{-k_1 t} - k_2 B(t) \tag{3}$$

since B is simultaneously generated from A and decaying by itself. The general solution of this linear ordinary differential equation has the form of

$$B(t) = \beta(t) e^{-k_2 t} \tag{4}$$

in which $\beta(t)$ is also a function of t. Taking (6) into (5) we have

$$\frac{\mathrm{d}B(t)}{\mathrm{d}t} = \beta'(t) e^{-k_2 t} - k_2 \beta(t) e^{-k_2 t} = k_1 A_0 e^{-k_1 t} - k_2 \beta(t) e^{-k_2 t} \tag{5}$$

so that

$$\beta'(t) = k_1 A_0 e^{-(k_1 - k_2)t} \tag{6}$$

and thus

$$\beta(t) = -A_0 \frac{k_1}{k_1 - k_2} e^{-(k_1 - k_2)t} + C \tag{7}$$

where C is a constant. Since B is not present at t=0 (time zero), but rather generated from A, therefore $B(t=0)=0$, so that

$$C = A_0 \frac{k_1}{k_1 - k_2} \tag{8}$$

and

$$B(t) = A_0 \frac{k_1}{k_1 - k_2} \left(1 - e^{-(k_1 - k_2)t}\right) e^{-k_2 t} = A_0 \frac{k_1}{k_1 - k_2} \left(e^{-k_2 t} - e^{-k_1 t}\right) \tag{9}$$

The rate of repopulation of GS is thus

$$\frac{\mathrm{d}G(t)}{\mathrm{d}t} = k_2 B(t) = A_0 \frac{k_1 k_2}{k_1 - k_2} \left(e^{-k_2 t} - e^{-k_1 t}\right) \tag{10}$$

from which it is easy to obtain the concentration of GS as function of t

$$G(t) = A_0 \left(-\frac{k_1}{k_1 - k_2} e^{-k_2 t} + \frac{k_2}{k_1 - k_2} e^{-k_1 t} \right) + D \tag{11}$$

where *D* is also a constant. At time zero, right after the photoexcitation, the concentration of GS is zero (completely excited). Therefore,

$$G(t) = A_0\left(-\frac{k_1}{k_1-k_2}e^{-k_2t} + \frac{k_2}{k_1-k_2}e^{-k_1t}\right) + A_0 \tag{12}$$

An apparent GSB recovery is formulated as

$$G(t) = A_0\left(1-e^{-k_{GSB}t}\right) \tag{13}$$

to make these two equivalent would require

$$\int_0^{+\infty} A_0\left(1-e^{-k_{GSB}t}\right)\mathrm{d}t = \int_0^{+\infty}\left(A_0\left(-\frac{k_1}{k_1-k_2}e^{-k_2t} + \frac{k_2}{k_1-k_2}e^{-k_1t}\right) + A_0\right)\mathrm{d}t \tag{14}$$

which gives

$$\frac{1}{k_{GSB}} = \frac{1}{k_1} + \frac{1}{k_2} \tag{15}$$

or

$$\tau_{GSB} = \tau_1 + \tau_2 \tag{16}$$

With τ_{GSB}=11 ps and $\tau_{^3MLCT}$ =9 ps in Figure 6, a τ_{MC}=2 ps could be estimated.